Engineering Ultrafast Carrier Dynamics at the Graphene/GaAs Interface by Bulk Doping Level

Jinghuan Yang, Quan Sun,* Wei Liu, Zhibin Zhang, Xiaoyong Hu,* Kaihui Liu,* Hong Yang, Hiroaki Misawa, and Qihuang Gong

Carrier dynamics, the most fundamental process in electronics and optoelectronics, has drawn great attentions owing to its crucial role in property engineering of materials. Exploration and regulation of carrier dynamics are essential for designing devices with specific functions and optimizing their performances. However, the lack of conventional tools with simultaneous ultrafast temporal and ultrasmall spatial resolution has impeded direct observation and manipulation of carrier dynamics at both the femtosecond and nanometer scale. In this study, the direct observation and modulation of ultrafast carrier dynamics at the graphene/gallium arsenide (GaAs) interface is achieved by tuning the doping level of bulk GaAs. This successful characterization is performed using advanced in situ photoemission electron microscopy combined with the ultrafast pump–probe technique. It is found that a change in the doping level in GaAs can change its band bending and switch the hot-carrier transfer direction at the graphene/GaAs interface with a lifetime reduction of nearly six times. This work paves the way of engineering ultrafast carrier dynamics at 2D interfaces by modifying the 3D bulk properties, and also provides a platform for fundamental studies of ultrafast physics with high spatial resolution.

Dr. J. Yang, Dr. W. Liu, Dr. Z. Zhang, Prof. X. Hu, Prof. K. Liu,
Prof. H. Yang, Prof. Q. Gong
State Key Laboratory for Mesoscopic Physics & Department of Physics
Collaborative Innovation Center of Quantum Matter
Beijing Academy of Quantum Information Sciences
Nano-optoelectronics Frontier Center of Ministry of Education
Peking University
Beijing 100871, P. R. China
E-mail: xiaoyonghu@pku.edu.cn; khliu@pku.edu.cn
Prof. Q. Sun, Prof. H. Misawa
Research Institute for Electronic Science
Hokkaido University
Sapporo 001-0021, Japan
E-mail: quansun@es.hokudai.ac.jp
Prof. X. Hu, Prof. H. Yang, Prof. Q. Gong
Collaborative Innovation Center of Extreme Optics
Shanxi University
Taiyuan, Shanxi 030006, P. R. China
Prof. H. Misawa
Center for Emergent Functional Matter Science
National Chiao Tung University
Hsinchu 30010, Taiwan

The carrier dynamics in different dimensions (space, time, and momentum) are important characteristics in exploring the nature of light–matter interactions and matter itself.[1–6] They play a decisive role in a variety of important technologies, including quantum computing, photoelectric devices, and bioengineering.[7–9] Based on hot-carrier directional transfer,[10] heterojunction cells can be formed in different semiconductors to realize highly efficient photovoltaic devices. In metal–semiconductor systems, the plasmonic energy conversion changes the energy distribution of excited electrons, thereby achieving electron–hole separation with high conversion efficiencies.[11–13] However, the lack of facile carrier-modulation methods renders the applications limited to specific materials without any flexibility. Hence, the manipulation of carriers to meet different application requirements has been a longstanding issue.

With the miniaturization of function devices, it is becoming hard to supply a sufficient description for the complex mechanism of carriers through macroscopic information, such as electrical current[14–16] and optical spectra.[17–20] Ultrafast relaxation processes and the ultrasmall spatial scale of carrier dynamics impede the use of most existing detection techniques. Thus, observing carriers directly in real space and imaging carrier dynamics with ultrafast temporal resolution remain considerable challenges. Until recent years, the technical progress brought about some breakthroughs in this field. Scanning ultrafast electron microscopy (SUEM), which combines electron microscopy with ultrafast lasers, enables the investigation of the spatiotemporal evolution of excited carriers.[21–23] Transient absorption microscopy (TAM), combining microscopy and transient absorption techniques, has also been reported for direct visualization of hot-carrier transport in hybrid perovskites.[24] Recently, photoemission electron microscopy (PEEM) has shown promising results in investigating hot carriers in multiple dimensions.[25–32] On the basis of electron microscopy, carriers in real space can be imaged directly with a high spatial resolution (<10 nm). Furthermore, in combination with pump and probe techniques, time-resolved PEEM can enable imaging of ultrafast carrier-dynamic processes.[33–35]

ADVANCED
SCIENCE NEWS
www.advancedsciencenews.com

ADVANCED
OPTICAL
MATERIALS
www.advopticalmat.de

Here, we report on the realization of engineering ultrafast carrier dynamics at the graphene/gallium-arsenide (GaAs) interface by tuning the bulk doping level. Based on PEEM, by integrating a two-color ultrafast pump–probe technique with a 300 fs temporal resolution, the surface hot-carrier dynamics can be imaged directly. In the graphene/GaAs sample, the excited electrons in graphene have a longer lifetime of 14.7 ps than those in GaAs (6.1 ps) and previously reported ones (2.4 ps) in a SiO_2 substrate.[36] However, in the graphene/n-GaAs sample, the situation reverses; the lifetime of the excited electrons in graphene reduces by nearly six times (2.6 ps). Low energy electron microscopy (LEEM) helps us to calibrate the direction of the band bending near the interface.[37–39] The LEEM results demonstrate that the existence of the substrate induces the mutual effect of hot carriers, which can influence the carrier dynamics of graphene. The downward band bending in the graphene/GaAs sample makes the GaAs an electron reservoir that provides an electron supply for graphene. On the other hand, the upward band bending in the graphene/n-GaAs sample offers an additional relaxation channel for the excited electrons in graphene. Furthermore, the unidirectional carrier transport at the interface, resulting from the band bending, also leads to the imbalance of carriers in graphene, which exacerbates the lifetime modulation. Consequently, we engineered ultrafast carrier dynamics at the interface in both temporal and spatial dimensions. This regulation of the lifetime of excited electrons in graphene should benefit many carrier-based applications.

We fabricated a graphene/GaAs sample by transferring single-crystal graphene prepared by chemical vapor deposition (CVD) onto a GaAs wafer by the polymethyl methacrylate (PMMA)-assisted method[40] (full details of the sample preparation are described in Note S1 in the Supporting Information). In our previous work,[41,42] we reported that the growth of centimeter-scale single-crystal graphene ensures the graphene is sufficiently large to cover the surface of the GaAs wafer. This sample was moved into an ultrahigh vacuum chamber where an excitation light illuminated the sample surface at normal incidence. When the photon energy was sufficiently high, electrons were emitted from the sample surface and escaped to the vacuum, where information about the surface was collected by PEEM (**Figure 1**a). Therefore, ultrahigh spatial resolution and nonscanning imaging was achieved. In terms of band structure, GaAs and graphene have a traditional semiconductor bandgap with a small bandgap energy of 1.42 eV and the unique gapless Dirac cones, as shown in Figure 1b. Therefore, these two materials have a wide range of applications in optoelectronic devices.[43,44] To investigate the hot-carrier dynamics on the surface of the graphene/GaAs sample, a two-color ultrafast pump–probe technique was integrated with PEEM. The femtosecond near-infrared pulses (800 nm, ≈100 fs) output from the femtosecond laser system were split to generate blue pulses (400 nm/3.11 eV) as the pump pulses and ultraviolet pulses (266 nm/4.66 eV) as the probe pulses with a time delay (details can be found in the Experimental Section). These two
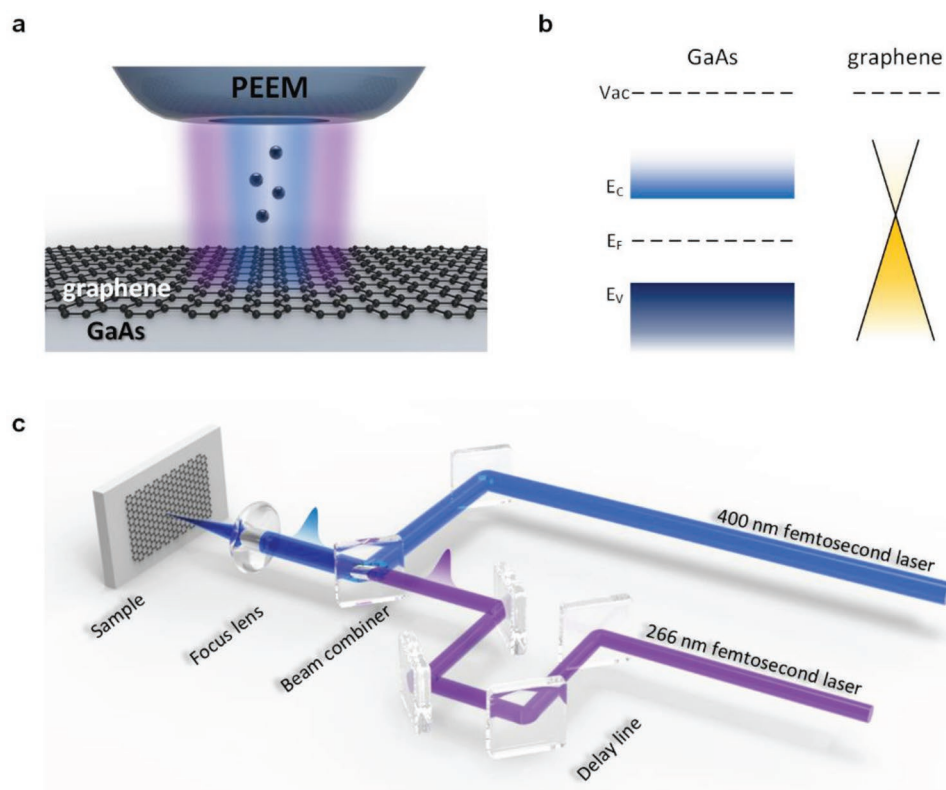
Figure 1. Schematic of PEEM with pump and probe setup and the band structure. a) Laser beams illuminated the graphene/GaAs sample vertically and photoemission electrons with surface information were collected by PEEM. b) The blue color represents the band structure of GaAs with a bandgap and the yellow color represents the gapless Dirac cone of graphene. c) Pump and probe setup. The blue beam represents the 400 nm pump laser and the violet beam represents the 266 nm probe laser with a time delay. These two beams were combined and focused on the sample surface.

1900580 (2 of 7)
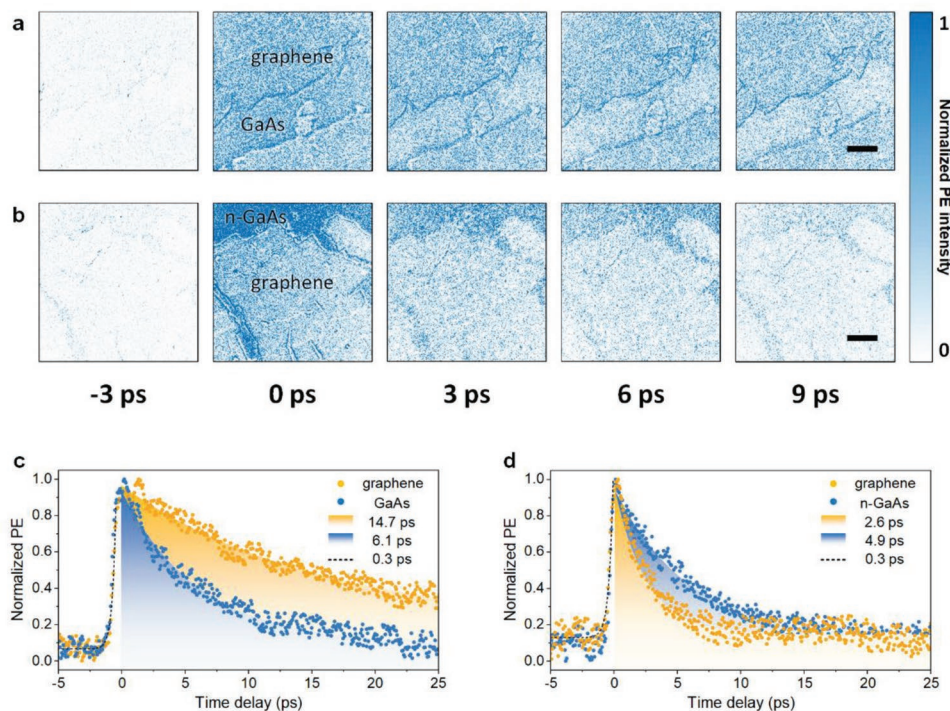
Figure 2. Carrier dynamics with different time delays in the real space and time-resolved evolution curves measured by PEEM. a) PEEM images recorded at different time delays for the graphene/GaAs sample. The background PE signal is subtracted from all images. The excited electrons in GaAs have a faster delay than those in graphene. The scale bar is 2 μm. b) PEEM images recorded at different time delays for the graphene/n-GaAs sample. Excited electrons in graphene have a faster delay than those in n-GaAs. The scale bar is 2 μm. c) Time-resolved evolution curves of the photoemission intensity reveal that excited electrons in graphene have a longer lifetime (14.7 ps) than those in GaAs (6.1 ps). The rising edges (dashed line) show a temporal resolution of ≈300 fs in our measurements. d) Time-resolved evolution curves of the photoemission intensity reveal that excited electrons in graphene have a shorter lifetime (2.6 ps) than those in GaAs (4.9 ps). The rising edges (dashed line) also show a temporal resolution of ≈300 fs in our measurements.

beams were combined and focused onto the sample surface (Figure 1c). In addition, because of the similar Fermi energies of graphene (≈4.6 eV)[45] and GaAs (≈4.78 eV),[46] the pump photon energy was not sufficient to emit electrons in both graphene and GaAs through a single-photon photoemission process. These electrons absorbed pump photons to become excited and occupied higher positions in the energy band. Excited electrons carrying different spatiotemporal information were emitted to the vacuum directly until the probe pulses reached the sample.

Based on this time-resolved PEEM system, the electron dynamics on the sample surface can be imaged directly with high spatial resolution. To compare the behavior of excited electrons on the GaAs and graphene surfaces, a crevice of graphene was chosen as the detection area. The surface morphology was imaged by scanning electron microscopy, as shown in Figure S3 in the Supporting Information. In addition, the 266 nm (Figure S4a,d, Supporting Information) and 400 nm pulses (Figure S4b,e, Supporting Information) can excite the background photoemission signal individually through a single- and two-photon photoemission process, respectively. This is verified by the slopes of the photoemission intensity curves against the excitation laser power (shown in Figure S4c,f, Supporting Information). Thus, the photoemission signal contributed by the excited electrons could be submerged with the background signal. To observe the evolution of the excited electrons clearly, the background photoemission signal was subtracted from all the images with different time delays shown in **Figure 2**a. Before the pump and probe pulses overlapped (−3 ps), no more electrons were excited except for the background signal and no extra photoemission signal was observed. These two pulses were then gradually overlapped; more electrons were excited by the pump pulse and a stronger signal was observed. The differences in the number of electrons excited in different materials enabled recognition of the surface morphology. With zero-time delay, a graphene crevice appeared in the PEEM image. Moreover, the stronger signal at the edge of graphene means a greater number of excited electrons trapped.[47] After the zero-time delay, owing to the electron–electron and the electron–phonon interactions, excited electrons with rapid relaxation caused the photoemission signal to become weaker. As the delay increased, the signals from GaAs became weak faster than those from graphene. The evolution of the photoemission signal contains the lifetime of excited electrons. It revealed qualitatively that excited electrons in graphene have a longer lifetime than those in GaAs. The complete dynamic processes are shown in Movie S1 in the Supporting Information. Furthermore, we integrated the photoemission intensity in GaAs and graphene, to plot the time-resolved evolution curves. Figure 2c shows that the lifetime of the excited electrons in GaAs was

6.1 ps and that of the excited electrons in graphene was 14.7 ps, which is much longer than previously reported values with an SiO_2 substrate.[36] Therefore, we deduce that the existence of GaAs induces the mutual effect of hot carriers at the interface and influences the carrier dynamics of graphene. In addition, similar rising edges (dashed line in Figure 2c) for these two materials were attributed to the temporal resolution of ≈300 fs in our measurements; the dynamics of the excitation process are hidden in the envelope of the pump and probe pulses.

To investigate the influence of the substrate on the carrier dynamics of graphene, we repeated the experiments described above with a graphene/n-GaAs sample. The electron dynamics on the surface was also recorded, as shown in Figure 2b. Before the pump and probe pulses overlapped (−3 ps), no electrons were excited and no extra photoemission signal was observed. With these two pulses overlapping, the surface morphology could be determined gradually. Unlike in the graphene/GaAs sample, the photoemission signal from n-GaAs was stronger. It is possible that the doping resulted in a smaller work function and higher electron density of n-GaAs. After the zero-time delay, the photoemission intensity also decreased rapidly. However, the signals from graphene became weak faster than those from n-GaAs. This indicates that the excited electrons in graphene have a shorter lifetime than those in n-GaAs. With a delay of 9 ps, the photoemission signal from both graphene and n-GaAs almost disappeared. The complete dynamic processes are shown in Movie S2 in the Supporting Information. The time-resolved evolution curves (Figure 2d) show that the lifetime of the excited electrons in n-GaAs was 4.9 ps and that of the excited electrons in graphene was only 2.6 ps, which was much shorter than that in the graphene/GaAs sample. Comparing these time-resolved evolution curves for graphene on GaAs and n-GaAs near the zero-time delay, some differences can be observed. In the graphene/n-GaAs sample, the photoemission intensity decreased immediately after the zero-time delay. On the other hand, in the graphene/GaAs sample, the photoemission intensity was maintained for ≈2 ps and then decreased. This phenomenon verifies our inference that the existence of the substrate induces the mutual effect of hot carriers at the interface and influences the carrier dynamics of graphene. Furthermore, we speculated that the lifetime of graphene would become longer as the doping level in n-GaAs decreased. However, due to current experimental conditions limitations, we do not have the ability to precisely control the doping level of n-GaAs experimentally. We will carefully study the effect of different doping levels on the electrons lifetime in future experiments. Nevertheless, different substrates resulted in different carrier dynamics of graphene. In our work, the change of the bulk doping level decreased the graphene electrons lifetime by nearly six times. Although, doping or defects introduced the mid-gap state for GaAs, the mid-gap state can only contribute with a small number of hot carriers. Therefore, the effect of the mid-gap state is small and cannot change the conclusion mentioned above.

Before exploring the nature of this phenomenon, we focus on the energy band at the interface between the graphene and the substrate. For the graphene/GaAs sample, the smaller work function of graphene compared to that of GaAs would guide electrons to flow from the graphene to the GaAs before the Fermi levels align. At equilibrium, a layer of positive charge would form in graphene and a layer of negative charge would form in GaAs. These two layers would establish an electric field at the interface. The low concentration of free carriers in GaAs cannot screen this electric field effectively. This causes the vacuum level and the energy band to bend near the interface[48–50] (Figure S5a, Supporting Information). Accordingly, we first used LEEM[37–39] to calibrate the difference of the vacuum levels between graphene and GaAs in situ. Details of the imaging principle of LEEM can be found in Note S2 in the Supporting Information. Quantitative contrast of the vacuum levels between graphene and GaAs can be obtained based on the reflected electron intensity curves against the electron energy when these electrons reached the sample surface.[51–53] These curves (**Figure 3**a) show that the reflected electron intensity of GaAs was higher than that of graphene on the falling edges. This means that the vacuum level of graphene was 0.24 eV lower than that of GaAs. As shown in Figure 3c, the difference in the vacuum levels generated the curved equipotential surfaces. Therefore, when incident electrons reached the surface of graphene, most of them were scattered, and a small number was reflected. While in GaAs, the incident electrons were all reflected above the surface. In this way, the intensity difference can be observed on the reflected electron intensity curves. In the same way, graphene and GaAs can be distinguished effectively from the high contrast of the electrons' reflected intensity derived from the difference of the vacuum levels (Figure 3d,e) in the LEEM image. Thus, the higher vacuum level of GaAs leads to a downward band bending in GaAs near the interface. On the other hand, for the graphene/n-GaAs sample, Figure 3b indicates that the reflected electron intensity of graphene was higher than that of n-GaAs on the falling edges. This means that the vacuum level of n-GaAs was 0.17 eV lower than that of graphene. In this case, the doping raised the Fermi level of GaAs and resulted in an upward band bending in n-GaAs near the interface (Figure S5b, Supporting Information). In real space, electrons reached the n-GaAs surface first (shown in Figure 3f) with fewer reflected electrons collected by the microscope. Correspondingly, the contrast of the LEEM image was reversed, as shown in Figure 3g,h, where the bright area represents graphene and the dark area represents n-GaAs. According to the above results measured by LEEM, the doping mainly changed the direction of the band bending which dominates the carrier transport between the graphene and the substrate.

The carrier dynamics can be described on the basis of the band structure with difference in band bending, as shown in **Figure 4**a,b. First, when the pump pulse reaches the surface of the sample, both graphene and GaAs absorb pump photons and generate electron–hole pairs. These high-energy electrons occupy high energy levels in the energy band. When the pump pulse goes through the material, the excited electrons relax to lower energy levels in the conduction band with electron–phonon interactions. Furthermore, this downward band bending accelerates the electron–hole separation near the interface and guides electrons in GaAs to relax to the gapless Dirac cone of graphene. In this filling behavior, GaAs acts as an electron reservoir with a steady supply of electrons. This explains the longer lifetime of the excited electrons in graphene compared to those in GaAs. Conversely, the holes in
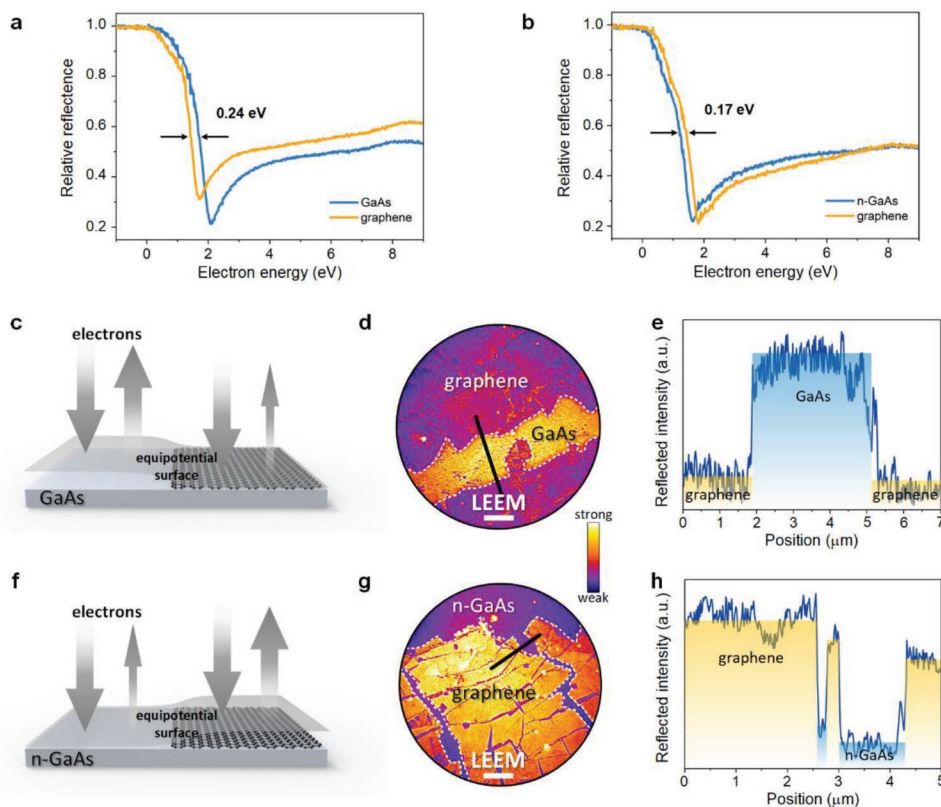
Figure 3. Surface morphology and difference of vacuum levels measured by LEEM. a,b) Reflected electron intensity curves against electron energy when the electrons reached the sample surface. The vacuum level of graphene (yellow line in (a)) is 0.24 eV lower than that of GaAs (blue line in (a)). The vacuum level of graphene (yellow line in (b)) is 0.17 eV higher than that of *n*-GaAs (blue line in (b)). c,f) Schematics of the LEEM imaging principle for the graphene/GaAs (graphene/*n*-GaAs) heterostructure. The difference of the vacuum levels originates from the bending of the equipotential surface above the sample surface. For the graphene/GaAs heterostructure, more electrons are reflected from the GaAs area; the graphene/*n*-GaAs heterostructure shows the opposite behavior. d,g) For the graphene/GaAs heterostructure, the bright area represents GaAs and the dark area represents graphene in the LEEM image. From the graphene/*n*-GaAs heterostructure, the contrast of LEEM image reverses. The scale bar is 2 µm. e,h) Reflected electron intensity curves along the black lines in (d) and (g).

graphene transfer to the GaAs along the direction of the band bending, except for those transferring to the top of the valence band. This unidirectional transfer causes an imbalance of the electrons and holes in graphene. Over time, this imbalance becomes more pronounced. Most of the holes in graphene are consumed and the rest of the electrons do not have a sufficient number of holes to recombine with. Hence, electrons supplemented from the bulk state and the imbalance of the electrons and holes in graphene contribute to the longer lifetime of the excited electrons in graphene. For the graphene/*n*-GaAs sample, the different band bending direction influences the carrier dynamics (Figure 4b). The upward band bending guides excited electrons to flow from graphene to *n*-GaAs. The additional relaxation channel accelerates the consumption of excited electrons in graphene. Moreover, holes in *n*-GaAs flow in the opposite direction, which contributes to the imbalance of electrons and holes in graphene. This increases the probability of recombination and accelerates the relaxation of excited electrons. Consequently, excited electrons in graphene have a shorter lifetime than those in *n*-GaAs. Compared with the graphene/GaAs sample, the lifetime of the excited electrons in graphene was reduced by approximately six times. Therefore, we demonstrated that the presence of the substrate influences the

carrier dynamics in graphene. Furthermore, by changing the bulk properties, we engineered the carrier-transport direction in the spatial dimension and modulated the electron lifetime.

Our realization of ultrafast carrier dynamics engineering at the interface will provide great flexibility in designing devices for different applications. Changing the bending direction of the bulk band at the interface by tuning the doping level can steer the hot-carrier transfer in the spatial dimension and change the lifetime of the excited electrons in graphene by nearly six times. This approach can be used to regulate the carrier properties of some existing materials. Furthermore, the direct and noninvasive imaging of the carrier dynamics by PEEM, with ultrafast temporal resolution and nanoscale spatial resolution, has the potential to offer a powerful platform for investigating new material systems and unique physical phenomena.

Experimental Section

Sample Preparation and Characterization: Centimeter-scale single-crystal graphene was prepared by a CVD method and was then transferred onto a GaAs wafer using a PMMA-assisted method (see Note S1 in the Supporting Information for details). SEM images of graphene on GaAs were acquired with a Zeiss electron microscope (Crossbeam 540) in
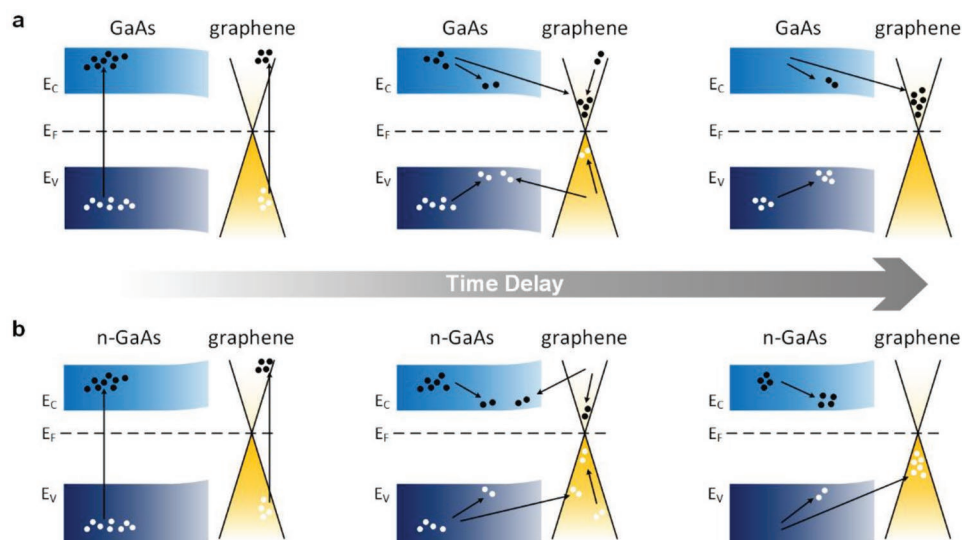
Figure 4. Carrier transport in the band structure with different time delays. a) Carrier dynamics of the graphene/GaAs sample with different time delays. At first, electrons are excited to high positions by the pump pulses. Hot carriers in both graphene and GaAs then relax to the bottom (top) of the conductive (valance) band. Owing to the downward band bending of the bulk band at the interface, electrons in GaAs transfer to graphene and holes in graphene transfer to GaAs. Over a long time, more electrons remain in the graphene without holes to recombine with. b) Carrier dynamics in the graphene/n-GaAs sample with different time delays. The upward band bending changes the direction of carriers transport. Electrons in graphene transfer to n-GaAs, whereas holes in n-GaAs transfer to graphene. Over a long time, electrons are consumed in the graphene with a short lifetime.

"inlens" mode operated at 3 kV. Before measurements, the graphene/GaAs and graphene/n-GaAs samples were outgassed and annealed at 350 °C for 12 h in an ultrahigh-vacuum chamber (below 5×10^{-9} Torr).

PEEM Measurements with Ultrafast Pump and Probe Technique: The measurements were based on a LEEM/PEEM system (SPELEEM, Elmitec GmbH), which enabled nonscanning and high-resolution imaging of electrons emitted from the samples surface (see Note S2 in the Supporting Information for details). In the pump and probe setup, the femtosecond near-infrared pulses (800 nm, ≈100 fs, 80 MHz) output from a Ti:sapphire femtosecond laser system (Mai Tai HP, Spectra-Physics) were split into two parts. The first part passed the femtosecond optical parametric oscillator (Inspire Auto 100, Spectra-Physics) to generate blue pulses (400 nm/3.11 eV). These blue pulses were then split again to be used as the pump pulses. The remaining blue pulses were combined with the second part of the 800 nm pulses to generate ultraviolet pulses (266 nm/4.66 eV) as the probe pulses with time delay. These two beams were combined and focused on the sample surface at normal incidence. Owing to the frequency doubling and the sum frequency, the pump and probe pulses were broadened and a temporal resolution of ≈300 fs was obtained.

Supporting Information

Supporting Information is available from the Wiley Online Library or from the author.

Acknowledgements

Conflict of Interest

The authors declare no conflict of interest.

Keywords

[1] S. Linic, P. Christopher, D. B. Ingram, *Nat. Mater.* **2011**, *10*, 911.
[2] D. Sun, G. Aivazian, A. M. Jones, J. S. Ross, W. Yao, D. Cobden, X. D. Xu, *Nat. Nanotechnol.* **2012**, *7*, 114.
[3] S. Gelinas, A. Rao, A. Kumar, S. L. Smith, A. W. Chin, J. Clark, T. S. van der Poll, G. C. Bazan, R. H. Friend, *Science* **2014**, *343*, 512.
[4] Y. Terada, S. Yoshida, O. Takeuchi, H. Shigekawa, *Nat. Photonics* **2010**, *4*, 869.
[5] R. Ulbricht, E. Hendry, J. Shan, T. F. Heinz, M. Bonn, *Rev. Mod. Phys.* **2011**, *83*, 543.
[6] W. Rehman, R. L. Milot, G. E. Eperon, C. Wehrenfennig, J. L. Boland, H. J. Snaith, M. B. Johnston, L. M. Herz, *Adv. Mater.* **2015**, *27*, 7938.
[7] C. H. Liu, Y. C. Chang, T. B. Norris, Z. H. Zhong, *Nat. Nanotechnol.* **2014**, *9*, 273.
[8] X. M. Wang, Z. Z. Cheng, K. Xu, H. K. Tsang, J. B. Xu, *Nat. Photonics* **2013**, *7*, 888.
[9] C. L. Yu, G. Li, S. Kumar, K. Yang, R. C. Jin, *Adv. Mater.* **2014**, *26*, 892.
[10] M. A. Green, S. P. Bremner, *Nat. Mater.* **2017**, *16*, 23.
[11] M. L. Brongersma, N. J. Halas, P. Nordlander, *Nat. Nanotechnol.* **2015**, *10*, 25.

**ADVANCED
SCIENCE NEWS**
www.advancedsciencenews.com

**ADVANCED
OPTICAL
MATERIALS**
www.advopticalmat.de

[12] C. Clavero, *Nat. Photonics* **2014**, *8*, 95.

[13] M. Taghinejad, H. Taghinejad, Z. H. Xu, Y. W. Liu, S. P. Rodrigues, K. T. Lee, T. Q. Lian, A. Adibi, W. S. Cai, *Adv. Mater.* **2018**, *30*, 1704915.

[14] L. Britnell, R. V. Gorbachev, R. Jalil, B. D. Belle, F. Schedin, A. Mishchenko, T. Georgiou, M. I. Katsnelson, L. Eaves, S. V. Morozov, N. M. R. Peres, J. Leist, A. K. Geim, K. S. Novoselov, L. A. Ponomarenko, *Science* **2012**, *335*, 947.

[15] M. S. Choi, G. H. Lee, Y. J. Yu, D. Y. Lee, S. H. Lee, P. Kim, J. Hone, W. J. Yoo, *Nat. Commun.* **2013**, *4*, 1624.

[16] X. Shi, K. Ueno, T. Oshikiri, Q. Sun, K. Sasaki, H. Misawa, *Nat. Nanotechnol.* **2018**, *13*, 953.

[17] Y. Yu, Z. H. Ji, S. Zu, B. W. Du, Y. M. Kang, Z. W. Li, Z. K. Zhou, K. B. Shi, Z. Y. Fang, *Adv. Funct. Mater.* **2016**, *26*, 6394.

[18] B. Y. Zheng, H. Q. Zhao, A. Manjavacas, M. McClain, P. Nordlander, N. J. Halas, *Nat. Commun.* **2015**, *6*, 7797.

[19] W. Li, J. Valentine, *Nano Lett.* **2014**, *14*, 3510.

[20] P. Wang, A. V. Krasavin, M. E. Nasir, W. Dickson, A. V. Zayats, *Nat. Nanotechnol.* **2018**, *13*, 159.

[21] O. F. Mohammed, D. S. Yang, S. K. Pal, A. H. Zewail, *J. Am. Chem. Soc.* **2011**, *133*, 7708.

[22] E. Najafi, V. Ivanov, A. Zewail, M. Bernardi, *Nat. Commun.* **2017**, *8*, 15177.

[23] E. Najafi, T. D. Scarborough, J. Tang, A. Zewail, *Science* **2015**, *347*, 164.

[24] Z. Guo, Y. Wan, M. J. Yang, J. Snaider, K. Zhu, L. B. Huang, *Science* **2017**, *356*, 59.

[25] K. Fukumoto, Y. Yamada, K. Onda, S. Y. Koshihara, *Appl. Phys. Lett.* **2014**, *104*, 053117.

[26] K. Keyshar, M. Berg, X. Zhang, R. Vajtai, G. Gupta, C. K. Chan, T. E. Beechem, P. M. Ajayan, A. D. Mohite, T. Ohta, *ACS Nano* **2017**, *11*, 8223.

[27] M. K. L. Man, A. Margiolakis, S. Deckoff-Jones, T. Harada, E. L. Wong, M. B. M. Krishna, J. Madeo, A. Winchester, S. Lei, R. Vajtai, P. M. Ajayan, K. M. Dani, *Nat. Nanotechnol.* **2017**, *12*, 36.

[28] S. Nemsak, E. Strelcov, T. Duchon, H. X. Guo, J. Hackl, A. Yulaev, I. Vlassiouk, D. N. Mueller, C. M. Schneider, A. Kolmakov, *J. Am. Chem. Soc.* **2017**, *139*, 18138.

[29] L. Wang, C. Xu, M. Y. Li, L. J. Li, Z. H. Loh, *Nano Lett.* **2018**, *18*, 5172.

[30] E. L. Wong, A. J. Winchester, V. Pareek, J. Madeo, M. K. L. Man, K. M. Dani, *Sci. Adv.* **2018**, *4*, eaat9722.

[31] J. H. Yang, Q. Sun, K. Ueno, X. Shi, T. Oshikiri, H. Misawa, Q. H. Gone, *Nat. Commun.* **2018**, *9*, 4858.

[32] G. Spektor, D. Kilbane, K. Mahro, B. Frank, S. Ristok, L. Gal, P. Kahl, D. Podbiel, S. Mathias, H. Giessen, F. J. Meyer zu Heringdorf, M. Orenstein, M. Aeschlimann, *Science* **2017**, *355*, 1187.

[33] Z. S. Chen, M. I. Lee, Z. L. Zhang, H. Diab, D. Garrot, F. Ledee, P. Fertey, E. Papalazarou, M. Marsi, C. Ponseca, E. Deleporte, A. Tejeda, L. Perfetti, *Phys. Rev. Mater.* **2017**, *1*, 045402.

[34] J. Kanasaki, H. Tanimura, K. Tanimura, *Phys. Rev. Lett.* **2014**, *113*, 237401.

[35] D. Niesner, H. Zhu, K. Miyata, P. P. Joshi, T. J. S. Evans, B. J. Kudisch, M. T. Trinh, M. Marks, X. Y. Zhu, *J. Am. Chem. Soc.* **2016**, *138*, 15717.

[36] K. Fukumoto, M. Boutchich, H. Arezki, K. Sakurai, D. Di Felice, Y. J. Dappe, K. Onda, S. Koshihara, *Carbon* **2017**, *124*, 49.

[37] L. Jin, Q. Fu, R. T. Mu, D. L. Tan, X. H. Bao, *Phys. Chem. Chem. Phys.* **2011**, *13*, 16655.

[38] K. Yan, D. Wu, H. L. Peng, L. Jin, Q. Fu, X. H. Bao, Z. F. Liu, *Nat. Commun.* **2012**, *3*, 1280.

[39] J. P. Shi, Y. Yang, Y. Zhang, D. L. Ma, W. Wei, Q. Q. Ji, Y. S. Zhang, X. J. Song, T. Gao, C. Li, X. H. Bao, Z. F. Liu, Q. Fu, Y. F. Zhang, *Adv. Funct. Mater.* **2015**, *25*, 842.

[40] X. Z. Xu, Z. H. Zhang, L. Qiu, J. N. Zhuang, L. Zhang, H. Wang, C. N. Liao, H. D. Song, R. X. Qiao, P. Gao, Z. H. Hu, L. Liao, Z. M. Liao, D. P. Yu, E. G. Wang, F. Ding, H. L. Peng, K. H. Liu, *Nat. Nanotechnol.* **2016**, *11*, 930.

[41] Z. B. Zhang, X. Z. Xu, Z. H. Zhang, M. H. Wu, J. H. Wang, C. Liu, N. Z. Shang, J. X. Wang, P. Gao, D. P. Yu, E. Wang, K. H. Liu, *Adv. Mater. Interfaces* **2018**, *5*, 1800377.

[42] X. Z. Xu, Z. H. Zhang, J. C. Dong, D. Yi, J. J. Niu, M. H. Wu, L. Lin, R. K. Yin, M. Q. Li, J. Y. Zhou, S. X. Wang, J. L. Sun, X. J. Duan, P. Gao, Y. Jiang, X. S. Wu, H. L. Peng, R. S. Ruoff, Z. F. Liu, D. P. Yu, E. G. Wang, F. Ding, K. H. Liu, *Sci. Bull.* **2017**, *62*, 1074.

[43] J. Yoon, S. Jo, I. S. Chun, I. Jung, H. S. Kim, M. Meitl, E. Menard, X. L. Li, J. J. Coleman, U. Paik, J. A. Rogers, *Nature* **2010**, *465*, 329.

[44] M. Chhowalla, D. Jena, H. Zhang, *Nat. Rev. Mater.* **2016**, *1*, 16052.

[45] R. S. Yan, Q. Zhang, W. Li, I. Calizo, T. Shen, C. A. Richter, A. R. H. Walker, X. L. Liang, A. Seabaugh, D. Jena, H. G. Xing, D. J. Gundlach, N. V. Nguyen, *Appl. Phys. Lett.* **2012**, *101*, 022105.

[46] J. S. Blakemore, *J. Appl. Phys.* **1982**, *53*, R123.

[47] C. G. Tao, L. Y. Jiao, O. V. Yazyev, Y. C. Chen, J. J. Feng, X. W. Zhang, R. B. Capaz, J. M. Tour, A. Zettl, S. G. Louie, H. J. Dai, M. F. Crommie, *Nat. Phys.* **2011**, *7*, 616.

[48] A. Di Bartolomeo, *Phys. Rep.* **2016**, *606*, 1.

[49] S. Tongay, M. Lemaitre, X. Miao, B. Gila, B. R. Appleton, A. F. Hebard, *Phys. Rev. X* **2012**, *2*, 011002.

[50] Z. Zhang, J. T. Yates, *Chem. Rev.* **2012**, *112*, 5520.

[51] P. L. Levesque, H. Marchetto, T. Schmidt, F. C. Maier, H. J. Freund, E. Umbach, *J. Phys. Chem. C* **2016**, *120*, 19271.

[52] Y. Murata, E. Starodub, B. B. Kappes, C. V. Ciobanu, N. C. Bartelt, K. F. McCarty, S. Kodambaka, *Appl. Phys. Lett.* **2010**, *97*, 143114.

[53] B. Unal, Y. Sato, K. F. McCarty, N. C. Bartelt, T. Duden, C. J. Jenks, A. K. Schmid, P. A. Thiel, *J. Vac. Sci. Technol., A* **2009**, *27*, 1249.

1900580 (7 of 7)